Advances in Environmental Technology 3 (2019) 157-169

Advances in Environmental Technology

journal homepage: http://aet.irost.ir

Removal of Ni (II) from aqueous solution using modified MCM-41 nano-adsorbents

Behrouz Raei[a]*, Afsaneh Barekat[b], Habibollah Shariatinia[a]

[a]*Department of Chemical Engineering, Mahshahr Branch, Islamic Azad University, Mahshahr, Iran*

[b]*Department of chemistry, Mahshahr Branch, Islamic Azad University, Mahshahr, Iran*

ARTICLE INFO

Article history:
Received 21 April 2020
Received in revised form
19 July 2020
Accepted 26 July 2020

Keywords:
Mesoporous MCM-41
Nano-adsorbent
Isotherm
Nickel

ABSTRACT

In this study, a synthetic and modified PPAP-MPTMS-MCM-41 nano-adsorbent was used to remove nickel (II) during a batch process. Studying the parameters that were effective on adsorption revealed that the PPAP-MPTMS-MCM-41 adsorbent was the most effective in the adsorption of nickel (II) from a standard solution (Conc. = 5 mg/L, volume = 100 mL) under the following conditions: pH=8, contact time = 20 min, 6 wt.% of poly para-aminophenol (PPAP) ligand, adsorbent mass = 0.3 g, 1 molar hydrochloric acid (to remove nickel from the adsorbent), and NaCl salt with a concentration of less than 100 g/L. The results showed that the Langmuir isotherm had a higher linear and non-linear fitting with the experimental data. Investigating the kinetic models and mass transfer of this adsorption process showed that the experimental data were in good agreement with the pseudo-second-order kinetic model and the intra-particle mass transfer model. According to thermodynamic studies, this adsorption process is endothermic; its Gibbs free energy value is positive such that with an increase in temperature, it goes to lower values, and thus the process progresses spontaneously.

1. Introduction

Nickel is usually present in nature in the form of oxide or sulfide. The most stable oxidation state of this metal is Ni^{+2}.Nickel is used in various industries such as alloying, steelmaking, and oil, as well as petrochemical industries (catalyst). This metal can be introduced into the environment during the mine exploration process by industries that deal with nickel compounds. As a result, it enters the body and leads to skin allergies and respiratory problems. An allergic reaction is the most common symptom in person's hypersensitive to nickel. The results of a study on factory workers who have dealt with nickel showed increased nickel concentrations in their blood, urine, and body tissues. Workers who inhale nickel suffer from asthma or dyspnea. Nickel toxicology studies show that workers who inhale large amounts of nickel suffer from other lung problems such as chronic bronchitis and decreased lung capacity [1].Therefore, it is important to control the amount of nickel in water, food, and bio-fluid. Different approaches have been developed for heavy metal removal including chemical precipitation, ion exchange, nano-filtration, reverse osmosis, and adsorption [2-4].The adsorption process is more popular than the other separation methods because of its simplicity, relatively low cost, and high efficiency. Batch adsorption studies were used to investigate the effect of adsorbent dosage, initial concentration of adsorbate, contact time, temperature, and pH on the removal of iron from pyrolyzed areca husk by Subramani et al. [5]. The adsorption capacity was found to increase with an increase in initial iron concentration and contact time but decreased with the adsorbent dosage. The Langmuir and Dubinin-Radushkevich models best describe the uptake of iron ions, implying monolayer adsorption with physisorption. The pseudo-second-order exhibited the best fit for the effectiveness of iron adsorption, indicating the

*Corresponding author. Tel: +989113209502
E-mail address: b.raei@mahriau.ac.ir
DOI: 10.22104/aet.2020.4178.1207

maximum limit of chemisorptions. Thermodynamic studies indicated that the adsorption was spontaneous and exothermic in nature. The adsorption of tetracycline on a modified zeolite was studied through a batch system by Jannat Abadi et al. [6]. Synthetic zeolite 13X was modified using Fe (III). The results showed that the removal efficiency of tetracycline by modified zeolite was considerably increased. The results indicated that tetracycline adsorption on the zeolite strongly depended on the pH of the solution due to amphoteric functional groups of tetracycline and maximum adsorption capacity of tetracycline by modified zeolite with a pH of approximately 6. The Langmuir isotherm showed good agreement with the experimental data suggesting monolayer adsorption. A straightforward procedure to synthesize keratin nanoparticles (KNP) from chicken feathers was established by Mousavi et al. [7]. The produced KNPs were then evaluated for the biosorption of Cu (II) from aqueous solutions. The analyzed adsorption isotherm data showed the change from a Redlich-Peterson isotherm to a Langmuir one by increasing the biosorbent dosage, which could be attributed to the more prepared adsorption sites. The experiments concerning the effect of the biosorbent dosage suggested the best removal at a KNP dose of 3.0 g/L.OSAC (granular activated carbon that was derived from olive oil industrial solid waste) were evaluated for their ability to remove phenol from aqueous solution by Sharaf El-deen et al. [8]. Adsorption isotherms were determined and modeled with five linear Langmuir forms, namely the Freundlich, Elovich, Temkin, Kiselev, and Hill-de Boer models. Adsorption was carried out on energetically different sites as localized monolayer adsorption and was an exothermic process. On the other hand, research on molecular sieves over the past few years has led to the production of new minerals called mesoporous molecular sieves. Mesoporous because of their regular channel structures that can be used in various fields such as catalysts, adsorption, molecular detection and separation, photocatalytic materials, chemical sensors, and optical devices [9-11].Researchers at the Mobil Company reported the synthesis of the Mesoporous Silica Molecular Sieve (M41S) family of mesoporous materials in 1992. One of the well-known members of the family is the MCM-41, which has a regular hexagonal structure with a similar open channel and a diameter in the range of 1.5 nm to 10 nm [12].The synthesis of the Mobil Composition of Matter (MCM-41) is associated with the formation of micelle in the water-surfactant system. In the structure of these materials, a surfactant is used as a template to synthesize mesoporous. The size and arrangement of the pores during the synthesis conditions are controlled by careful selection of surfactants. Øye et al. [13] well described the details of the synthesis of mesoporous materials. The high surface area of the MCM-41 and its mesoporous structure provides good support for a large number of chemical ligands with large dynamic diameters. The hydrophobic and hydrophilic properties and structural modifications of MCM-41 have led to its use as an adsorbent for adsorption of various species. MCM-41 has significant features: 1) the specific porous structure with pores with diameters of 15 Å to 100 Å, which can be controlled by careful selection of surfactants, primary chemicals, and other parameters, 2) high thermal stability, which leads to the expansion of its application, and 3) a high surface area. These are the reasons for using MCM-41 as advanced adsorbent and molecular sieve. Several studies have been conducted on the use of modified amorphous silica with various functional groups in the field of heavy metal adsorption. Different types of functional groups and different molecules can be housed in the MCM-41 host structure. For example, thiol functionalized silica exhibits selective binding ability for Hg(II) in coexistence with other metal ions [14]. Thiol and amino functionalized SBA-15 silica were used by Liu et al. for removal of Hg (II), Cu (II), Zn (II), Cr (III) and Ni (II) [15].But, in most studies to remove nickel (II) ions, the MCM-41 adsorbent has been modified by amino and imine agents such as Aminopropyl [16], pyridine [17] Diethylenetriamine [18] Polyethylenimine [11] and Ethanediamine [19].According to these studies, it can be concluded that the modified adsorbent has a much higher adsorption and efficiency capacity than the mesoporous non-modified adsorbent and adsorbents such as activated carbon, silica gel, and cellulose. A summary of the research on the modification of MCM-41 for adsorption of nickel (II) ions is given in Table 1.

Table 1. Adsorption of nickel (II) by modified MCM-41 nano-adsorbent with various agents

	Modified agent of MCM-41	Reference
1	Amino-propyl	[16]
2	Acetylacetone	[20]
3	Pyridine	[17]
4	Poly- Para-Aminophenol	[21]
5	Diethylenetriamine	[18]
6	Polyethylenimine	[11]
7	Ethanediamine	[19]

In this study, a new adsorbent was prepared by the modification of calcinated MCM-41 with 3-mercaptopropyltrimethoxysilane (MPTMS) and electro-reduction product of 4-nitrophenol (PPAP). The PPAP is a new Ni(II) selective chelating agent (polymer), which was synthesized by PPAP in an acetate medium [22]. This polymer, which is a new kind of polyaminophenol, has a high tendency to form a complex with Ni(II) [22].So, first, MPTMS-MCM-41 and PPAP- MPTMS-MCM-41 were obtained, respectively. Then, the modified adsorbent in the nickel (II) adsorption process was used in a batch process and after investigating the effect of various factors including ligand mass, pH, contact time, adsorbent mass, hydrochloric acid concentration, and ionic strength, the optimal value of

these parameters was obtained. The main objective of this study was to investigate the kinetic and thermodynamic model and mass transfer mechanism of this adsorption process.

2. Materials and methods

2.1. Chemicals and reagents

The following listed items were all purchased from Merck (Germany): 4-Nitrophenol, cetyltrimethylammonium bromide (CTAB), tetraethylorthosilicate (TEOS), aqueous ammonia (25% w/w), ethanol (96%), methanol, sodium acetate trihydrate, and common chemicals such as hydrochloric acid, phosphoric acid, and sodium hydroxide. The MPTMS (99%) was purchased from Sigma Aldrich. the nickel standard stock solution was obtained from Carl Roth GmbH (Germany). The working standard solutions were made daily by stepwise dilution of the standard stock solution with ultra pure water. The buffer solutions (0.5 mol/L, pH = 7) were prepared from phosphoric acid and sodium hydroxide solutions. All the chemicals were of analytical grade and used without further purification.

2.2 Methods

2.2.1 Synthesis and calcination of MCM-41 mesoporous

A rapid method was implemented for the synthesis of MCM-41 [23].For this purpose, the surfactant CTAB was dissolved in a mixture of water (155 mL)/ethanol, and then the ammonia solution and sodium acetate were added. After about 10 min of stirring at 200 rpm, a clear solution was acquired. Then, the TEOS was added immediately to this solution. The final molar ratio of the resulting gel composition was TEOS: 1; CTAB: 0.22; sodium acetate: 0.034; NH_3: 11; ethanol: 1; and water: 155. After 2.5 h of stirring at room temperature, the obtained gel was transferred to a Teflon-lined stainless steel vessel and aged at 70°C for 5 h. Finally, the white precipitate was filtered and washed with copious amounts of water. The resulting surfactant containing MCM-41 was dried at 70°C for 3 h and then calcinated in an air atmosphere at a heating rate of 5°C min^{-1} up to 550°C (held at this temperature for 5 h) [24].

2.2.2 **Modification of calcinated-MCM-41**

In this work, the post-synthesis route was chosen for the chemical modification of calcinated MCM-41 by MPTMS [25]. The calcinated MCM-41 (0.5 g) was dispersed in 100 mL of dry toluene at 60°C. After 30 min of stirring at 350 rpm, 2 mL of MPTMS was added. The mixture was stirred at 60°C for 6 h and then filtered; the resulting modified material was washed with 100 mL of toluene. The MPTMS-MCM-41 was dried at 70°C for 3 h and then left for characterization. After the characterization of the MPTMS-MCM-41, the incorporation of the Ni (II) selective chelating agent was carried out in a water/methanol (1:1) mixture. In this procedure, the Ni(II) selective chelating agent (20 mg as an optimum amount) was dissolved in15 mL of methanol. Then 0.5 g of MPTMS-MCM-41 was dispersed in 15 mL of water. Lastly, two solutions were mixed and agitated at ambient temperature for 6 h. The resulting PPAP-MPTMS-MCM-41was filtered, washed with ultra pure water, and then dried at70°C for 3 h [24]. Finally, the nickel (II) selective adsorbent of PPAP-MPTMS-MCM-41 (4.0 w/w) was used to extract and absorb nickel ions by the batch process.

2.2.3 Adsorbent characterization

The SEM images of the calcinated MCM-41 are shown in Figure 1. The particle morphology of the MCM-41 is variable. The particle size ranges from approximately 40 to 100 nm. Nevertheless, some particles larger than 100 nm can be seen in the SEM images.

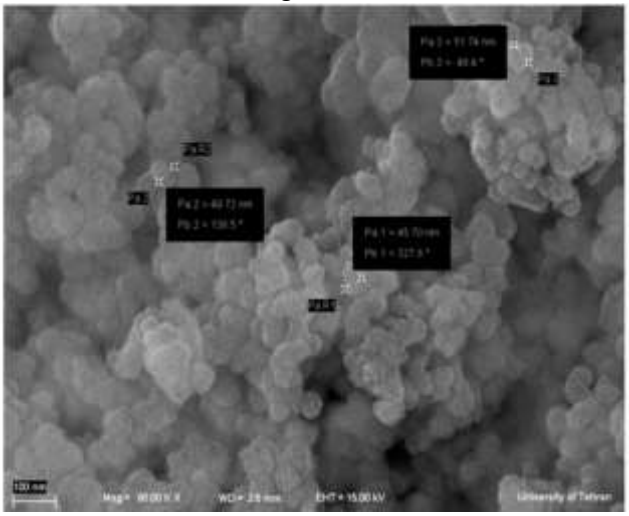

Fig. 1. SEM micrographs of calcined MCM-41

The nitrogen adsorption-desorption isotherms for MCM-41 are shown in Figure 2. They all displayed type IV isotherms. The volume of nitrogen adsorbed decreased with functionalization, which is indicative of a reduction in pore size. The BET specific surface area, pore volume, and average pore diameters of the MCM-41 were calculated using the Barrett–Joyner–Halenda model of the adsorption branch (Table 2). As can be seen, the BET surface area and total pore volume decreased after chemical modification and incorporation. Because the mercaptopropyle chains were grafted to the surface of the hexagonal channels, it facilitated the strong incorporation of the PPAP via SH-NH interactions [24].

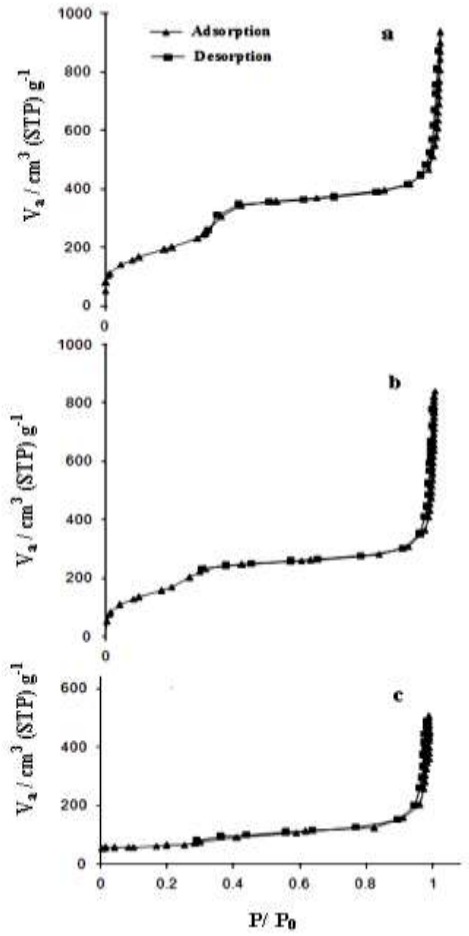

Fig. 2. The nitrogen adsorption–desorption isotherms a) Calcinated MCM-41 b) MPTMS-MCM-41 c) PPAP-MPTMS-MCM-41

Table 2. Structural parameters of the mesoporous samples.

Adsorbent	BET surface area (m^2/g)	Pore volume (cm^3/g)	Pore diameter (nm)
Calcinated MCM-41	864	1.4	6.51
MPTMS-MCM-41	723	1.23	6.23
PPAP-MPTMS-MCM-41	422.6	0.85	5.24

2.2.4. Adsorption isotherm

The adsorption isotherm models expressed the interaction between the Ni (II) and the adsorbent. The following equation could be applied to calculate the adsorption capacity of Ni (II) at equilibrium [26]:

$$q_e = \frac{(C_0 - C_e)V}{m} \quad (1)$$

The removal of Ni (II) was calculated according to the following equation[26]:

$$R\% = \frac{(C_0 - C_e)}{C_0} \times 100 \quad (2)$$

where C_0 and C_e (mg/L) are the initial and equilibrium concentrations of Ni(II), respectively, V(L) is the volume of the solution, and m (g) is the mass of absorbent.

2.2.4.1. Freundlich isotherm

The Freundlich isotherm model, which is an empirical model, can be expressed by the following relationship[27]:

$$q_e = K_F C_e^{\frac{1}{n}} \quad (3)$$

where K_F (mg/g) and n are the Freundlich constants related to the adsorption capacity and intensity, respectively.

2.2.4.2. Langmuir isotherm

The Langmuir model is represented by Eq. (4) [28]:

$$q_e = \frac{k_l q_m C_e}{1 + q_m C_e} \quad (4)$$

where q_e denotes the amount of metal adsorbed per unit mass of adsorbent (mg/g), C_e shows the nickel concentration at equilibrium (mg/L), K_l is Langmuir constant (L/g), and q_m is the maximum adsorption capacity of the adsorbent (mg/g).

2.2.4.3. Temkin isotherm

The Temkin model investigates the effect of some indirect interactions of adsorbent-adsorbate on the adsorption isotherm. This model assumes that the adsorption heat of all the molecules in the adsorbed layer is reduced by adsorbent-adsorbate interactions, and adsorption is described by the uniform distribution of bonding energies [29].The Temkin equation is expressed as Eq. (5):

$$q_e = \frac{RT}{b} \ln(K_T C_e) \quad (5)$$

where T is the absolute temperature, R is the universal gas constant and is equal to 8.314 J mol^{-1} K^{-1}, K_T (L/mg) is the equilibrium bonding constant, and b (kJ/mol) is the change of adsorption energy.

2.2.4.4. Dubinin-Radushkevich isotherm

This model was first proposed for the adsorption of gases under critical conditions on porous solids with microspores:

$$q_e = Q_s \exp(-K_{ads} \varepsilon^2) \quad (6)$$

This isotherm is in good accordance with the data and is commonly used to determine the physical and chemical adsorption of metal ions using their mean free energy (E):

$$E = \frac{1}{\sqrt{2B_{DR}}} \quad (7)$$

where B_{DR} is the constant isotherm or K_{ads}, which is related to the energy required to move any molecule absorbed from an infinite distance to the adsorbent surface (mol^2 KJ^{-2}). The parameter ε is equivalent to the potential energy and is defined by Eq. (8) [29]:

$$\varepsilon = RT \ln\left[1 + \frac{1}{C_e}\right] \quad (8)$$

2.2.4.5. Redlich-Peterson isotherm

The Redlich-Peterson isotherm is a three-parameter model that incorporates the features of the Langmuir and Freundlich isotherms. This model can be represented as Eq. (9) [30]:

$$q_e = \frac{K_{RP} C_e}{1 + \alpha_{RP} C_e^{\beta_{RP}}} \quad (9)$$

where K_{RP} (L/mg), a_{RP}, and β_{RP} are Redlich-Peterson constants. When the value of $a^{RP}C_e{}^{\beta RP}$ is much greater than 1 (β_{RP} tends to zero), this isotherm reduces to the Freundlich model. It also reduces to the Langmuir isotherm in the cases where β_{RP} approaches to 1.

2.2.4.6. Sips isotherm

The Sips equation includes three parameters and is a combination of the Langmuir and Freundlich isotherms, which can be expressed as Eq. (10) [31]:

$$q_e = \frac{K_s C_e^{\beta}}{1 + a_s C_e^{\beta}} \quad (10)$$

where K_S (Lm/g), a_S, and β are Sips constants. The equation reduces to the Langmuir isotherm when β is 1, and it reduces to the Freundlich isotherm at low concentrations of the adsorbate.

2.2.5. Adsorption kinetics

To investigate the mechanism of adsorption, the kinetic data for the sorption of Ni^{+2} ions onto the adsorbent were analyzed using first-order, pseudo-second-order, and diffusion kinetic models.

2.2.5.1. First and pseudo-second-order kinetic models

Zeldowitsch studied the adsorption of carbon monoxide on manganese dioxide and concluded that the adsorption rate of carbon monoxide decreases exponentially as the amount of gas absorbed increases. Elovich formulated the results of Zeldowitsch's work in the following equation [32]:

$$\frac{dq}{dt} = \alpha e^{-\beta q} \quad (11)$$

where q is the amount of gas absorbed at time t, α is the initial velocity, and β is the removal constant in each experiment. By assuming $\beta\alpha t \gg 1$ (to simplify the equation) and applying the boundary conditions, Eq. (11) turns into Eq. (12):

$$q = \beta \, \mathrm{Ln}\,(\alpha\beta) + \beta \, \mathrm{Ln}\, t \quad (12)$$

The second-order velocity equation for soluble species is written in terms of the adsorbent adsorption capacity at different times and thus is called the pseudo-second-order kinetic. The velocity of the second-order reaction depends on the concentration of nickel ion adsorbed on the adsorbent and the equilibrium concentration of nickel ion in the solution. Therefore, the velocity relation can be written in terms of the positions occupied at equilibrium time (P_e) and the positions occupied at time t (P_t):

$$\frac{dP_t}{dt} = k[P_e - P_t]^2 \quad (13)$$

Given that the difference in equilibrium adsorption capacity and adsorption capacity at time t (q_e-q_t) indicates the active and ready-to-accept positions of the ions, the above kinetic relationship (Eq. 13) can be written as follows.

$$\frac{dq_t}{dt} = k[q_e - q_t]^2 \quad (14)$$

where the constant k indicates the adsorption velocity constant (g mg^{-1} min^{-1}). By applying the boundary conditions, the kinetic relation is expressed as Eq. (15).

$$\frac{t}{q} = \frac{1}{h} + \frac{1}{q_e} t \quad (15)$$

where h is the initial velocity of the adsorption ($h = k\, q_e^2$), indicating a case where the ratio of t⁄q tends to 0 [32].

2.2.5.2. Intra-particle diffusion model

Three steps control the processes of adsorption of the metal ions by the adsorbents: 1) Transferring metal ions from the joint film between the solution and the adsorbent to the adsorbent surface;2) Transferring the ions (here nickel ions) from the surface of the adsorbent or nano-adsorbent particles to the intra-particle active sites; and 3)The adsorption of ions by these active sites via ion exchange reaction or the formation of stable complexes between metal ions and ion exchange groups or between metal ions and complexing functional groups[33]. According to Weber and Moris, the initial velocity of intra-particle penetration is expressed as follows [32]:

$$q_t = k_d . t^{0.5} \quad (16)$$

where q_t (mg/g) is the amount of metal ions adsorbed on the adsorbent at time t and k_d is the ion penetration coefficient in the adsorbent solid network (mgg^{-1} $min^{-1/2}$).

3. Results and discussion

3.1. Investigation of adsorption efficiency

In this step, three standard 100 ml solutions containing nickel (II) with a concentration of 5mg/L were prepared. About 0.2 g of each of the calcined MCM-41, MPTMS-MCM-41, and PPAP-MPTMS-MCM-41 adsorbents was added to each of the above solutions. To prepare the PPAP-MPTMS-MCM-41 adsorbent, 20 mg PPAP was loaded on 0.5 g of MPTMS-MCM-41 adsorbent so that the adsorbent containing 4 wt.% of PPAP ligand (PPAP-MPTMS-MCM-41 (4.0 ww^{-1}) was obtained. The adsorption process of each solution was performed for 30 min, and the solution was stirred at a rate of 300 rpm. The centrifugation was executed for 5 min at 3000 rpm; the adsorbent containing the nickel absorbed was separated, and the supernatant was discarded. The separated adsorbent was first rinsed with 10 ml of distilled water and then with 1 ml of 2 molar

chloride acid to remove the nickel from the adsorbent. After stirring the test tube with a gentle motion of the hand for 5 min, centrifugation was performed again, and the acidic solution containing the removed nickel was separated and injected into the ICP-OES device. Finally, to assess the ability of the adsorbents in nickel (II) absorption, the nickel emission intensity at a wavelength of 221.647 nm was measured by the ICP-OES device. The results for these three adsorbents are shown in Table 3. According to Table 3, the higher emission rate confirms the prominent role of the PPAP ligand, and therefore the adsorbent (PPAP-MPTMS-MCM-41 (4.0 w/w)) selected in the adsorption of the nickel (II) ions.

Table 3. The ability of different adsorbents in nickel(II) adsorption

Adsorbent	Emission intensity
MCM-41Calcined	94186
MPTMS-MCM-41	183251
PPAP-MPTMS-MCM-41	281753

The experiments were performed by one factor at a time method. At each step, the changes in one of the parameters in Table 4 were investigated. Some parameters were also considered constant, as shown in Table 5.

Table 4. Parameters examined for nickel (II) adsorption by PPAP-MPTMS-MCM-41

	Parameter	Range	Unit
1	Mass of PPAP on MPTMS-MCM-41	5-50	mg
2	pH	2-12	-
3	Contact time	5-60	min
4	Adsorbent mass	0.1-0.5	g
5	HCl concentration	0.1-2	mol/L
6	Ionic strength (NACL)	0-150	g/L

Table 5. Values of constant parameters considered in nickel (II) adsorption

Parameter	Quantity	Unit
Ni(II) Concentration	5	mg/L
Centrifugation time	5	min
Centrifugation speed	3000	rpm
Initial volumes of samples	100	ml
HCL(elution) volume	1	ml

3.1.1 The effect of PPAP ligand mass loaded on MPTMS-MCM-41 adsorbent

To study the effect of the PPAP ligand mass loaded on 0.5 g of MPTMS-MCM-41adsorbent, 5 to 50 mg of ligand mass were used. Following the adsorption of the nickel (II) ions and their removal from the hydrochloric acid medium, the emission intensity at a wavelength of 221.647 nm was traced. The results (Figure 3) show that the adsorbent efficiency increases with increasing ligand mass to 30 mg (6 wt.%) and then remains almost constant. For this reason, in subsequent experiments, the PPAP-MPTMS-MCM-41 (6.0 w/w) adsorbent was used as the optimal adsorbent.

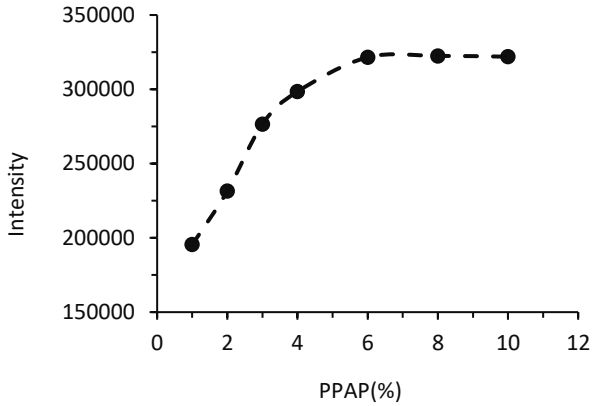

Fig.3. The effect of PPAP percentage loaded on MPTMS-MCM-41adsorbent

3.1.2. PH effect

The effect of pH on the adsorption efficiency of PPAP-MPTMS-MCM-41 (6.0 w/w) in the nickel (II) ions adsorption was performed at pH values of 2, 4, 6, 7, 8, 9, 10, and 12. In this study, the nickel emission line intensity at a wavelength of 221.647 nm after the removal of nickel (II) from the PPAP-MPTMS-MCM-41 (6.0 w/w) adsorbent was investigated by 2 molars hydrochloric acid as a function of the pH of the primary solution. The results (Figure 4) show that with increasing pH to 8, the emission intensity (as an indicator of adsorption efficiency in nickel (II) ion extraction) increases while it decreases at a pH greater than 8. The decreased complex formation at a pH less than 8 and the formation of nickel hydroxide at a pH greater than 8 are the most important factors in reducing the adsorption efficiency in acidic and alkaline environments. Therefore, a pH = 8 was selected as the optimal value of this parameter in subsequent experiments.

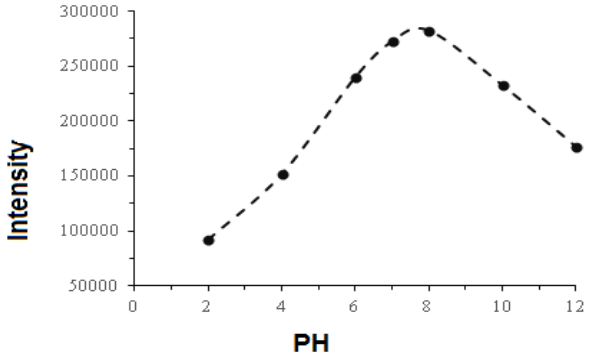

Fig. 4. The effect of pH on the efficiency of PPAP-MPTMS-MCM-41 (6.0 w/w) adsorbent

3.1.3 Effect of contact time

To investigate the effect of the contact time of the PPAP-MPTMS-MCM-41 (6.0 w/w) adsorbent, solutions containing small amounts of nickel (II) with a concentration of 5 mg/L

at a time range of 5 to 60 min were studied. Figure 5 shows that the adsorbent has relatively rapid absorption kinetics and reaches equilibrium after 20 min. Therefore, 20 min was used in subsequent experiments as the optimal contact time.

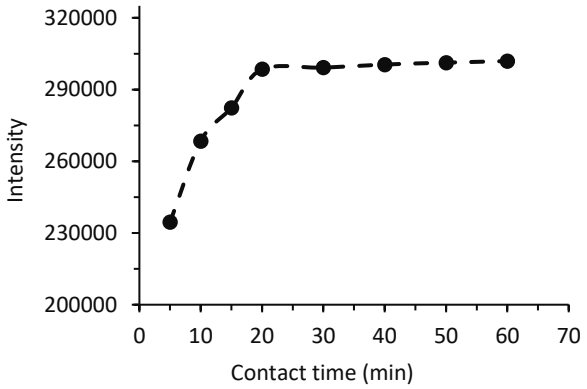

Fig. 5. The effect of contact time on the efficiency of PPAP-MPTMS-MCM-41 (6.0 w/w) adsorbent

3.1.4 Effect of PPAP-MPTMS-MCM-41 (6.0 w/w) adsorbent mass

Experiments were performed using the adsorbent mass in the range of 0.1 to 0.5 g to obtain the optimal mass of the synthetic nano-adsorbent containing 6% PPAP ligand. The results of drawing the nickel emission intensity versus the adsorbent mass are shown in Figure 6. As can be seen, the highest efficiency is obtained in the mass range of 0.3 to 0.5 g. Therefore, a mass of 0.3 g was preferred in subsequent experiments.

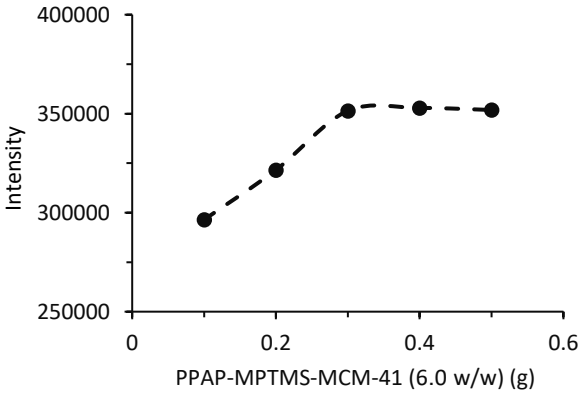

Fig.6. The effect of PPAP-MPTM-MCM-41 (6.0 w/w) adsorbent mass on nickel (II) adsorption

3.1.5 Effect of chloride acid concentration

To remove the adsorbed nickel from the adsorbent and revive the adsorbent for subsequent use, 1 ml of hydrochloric acid with concentrations of 0.1 to 2 molar was used. Due to the low stability of the nickel complex (II) with the PPAP ligand in acidic environments (pH less than 4), it was thought that washing with hydrochloric acid completely removed the nickel (II) ions from the adsorbent. According to Figure 7, to achieve optimal performance, the concentration of hydrochloric acid consumed in the nickel removal phase must be at least 1 molar or more. However, due to the structural and chemical instability of the MCM-41 mesoporous nano-adsorbent in highly acidic environments, 1 molar hydrochloric acid was preferred for use in subsequent experiments.

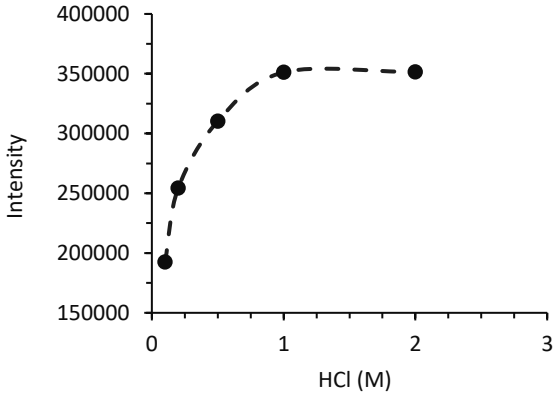

Fig.7. The effect of the concentration of hydrochloric acid used to remove nickel (II) absorbed by the PPAP-MPTM-MCM-41 (6.0 w/w) adsorbent

3.1.6 Effect of ionic strength

Because most industrial water environments have a high salt content, the ability of adsorbent in nickel (II) ions adsorption from environments with different ionic strengths was investigated. Since sodium chloride is the most abundant salt in these environments, this study was conducted in the range of 0 to 150 g/L of sodium chloride. The emission intensity of the nickel absorbed from the salt medium in the 1 molar hydrochloric acid was plotted as a function of the salt concentration in Figure 8. The results showed that there was no significant relationship between adsorbent efficiency and ionic strength at concentrations of less than 100 g/L. At higher concentrations, adsorption efficiency is likely to decrease due to severe ionic interactions.

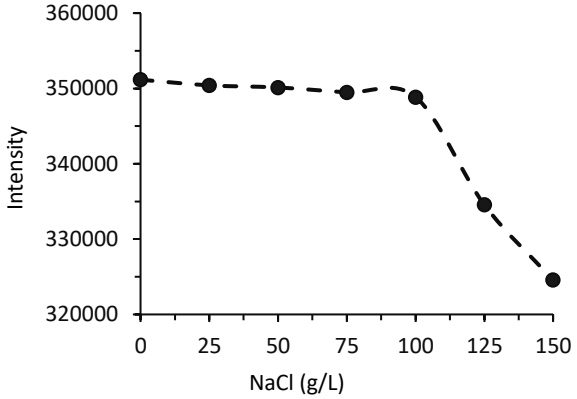

Fig. 8. The effect of ionic strength on the efficiency of PPAP-MPTM-MCM-41 (6.0 w/w) adsorbent

Table 6 shows the optimal conditions for the parameters affecting the process of nickel (II) ion adsorption by the

PPAP-MPTMS-MCM-41 mesoporous adsorbent. In the following, kinetic, thermodynamic, and mass transfer studies were conducted under these optimal conditions.

Table 6. Optimal conditions for extraction of nickel (II) by PPAP-MPTMS-MCM-41 nano-absorbent

Parameter	Optimum value	Unit
pH	8	-
Contact time	20	min
%PPAP	6	%
Adsorbent mass	0.3	g
HCL concentration	1	mol/L
NaCl concentration	<100	g/L

3.2. Adsorption isotherm

The parameters of the Langmuir, Freundlich, Dubinin-Radushkevich, and Temkin isotherms, also known as two-parametric isotherms, were obtained by plotting the corresponding curves through the slope and width of the intercept of the graphs. The drawn graphs and the calculated parameters are shown in Figure 9 and Table 7, respectively.

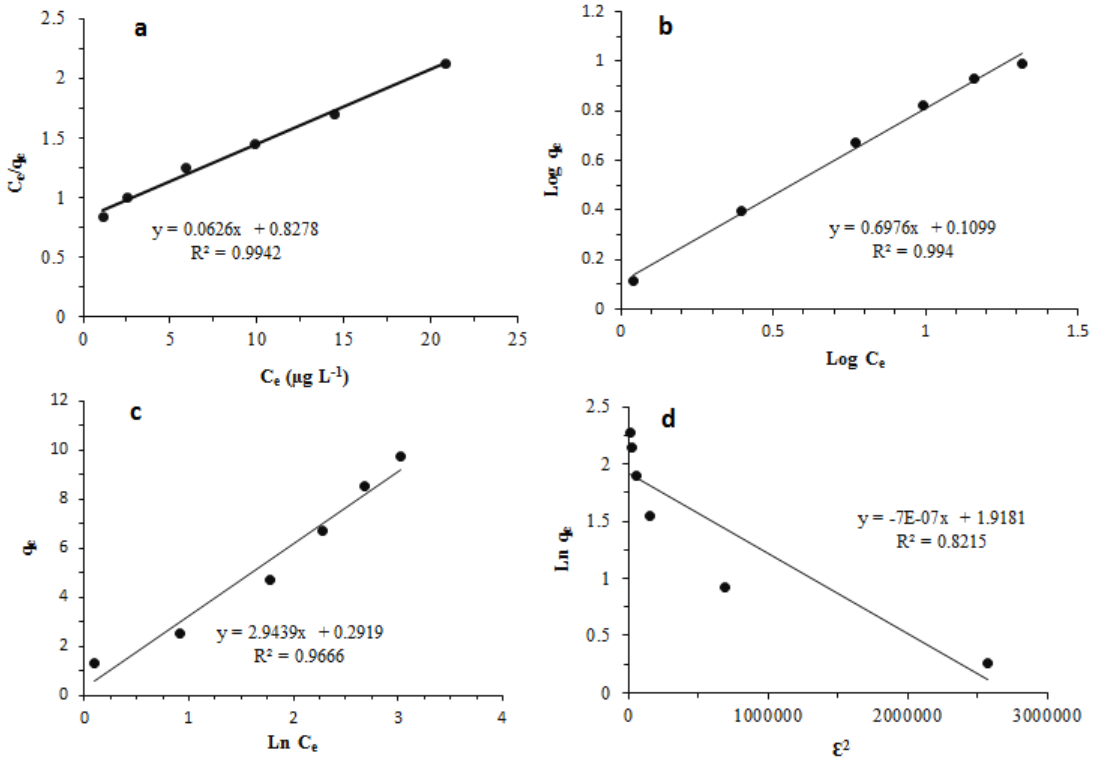

Fig. 9. The fitting of the linear form of the (a)Langmuir, (b) Freundlich, (c) Temkin, and(d) Dubinin-Radushkevich isotherms with experimental data

As expected, the linear fitting of the Langmuir isotherm with the experimental data is greater. This greater consistency is because the important assumptions of this isotherm are homogeneity or uniformity of the adsorption sites, the absence of adjacent interactions, and the monolayer of the adsorbed species. These assumptions are preludes to chemical adsorption, which is the most probable form of adsorption for PPAP-MPTMS-MCM-41 nano-adsorbent in the adsorption of nickel (II) ions.The importance of this adsorbent is attributed to the use of MPTMS and PPAP in its structure, the first of which is mostly used to stabilize PPAP in the structure. PPAP plays an important role in the adsorption process by having functional groups (-NH and –OH) as selective ligands in the formation of stable complexes with nickel (II) ions [24].Therefore, the surface of the adsorbent is prone to a favorable chemical interaction (chemical adsorption) with nickel ions. The Redlich-Peterson and Sips have three parameters or constants that are unknown. Curve fitting of the experimental data was used to obtain these constants (Table 8). The linear equation of these isotherms was calculated and plotted as some graphs (Figure 10). The results indicate that the behavior of these isotherms also has good linear regression because these equations in these conditions tend to Langmuir behaviors. This also confirms the possibility of chemical adsorption mechanisms.

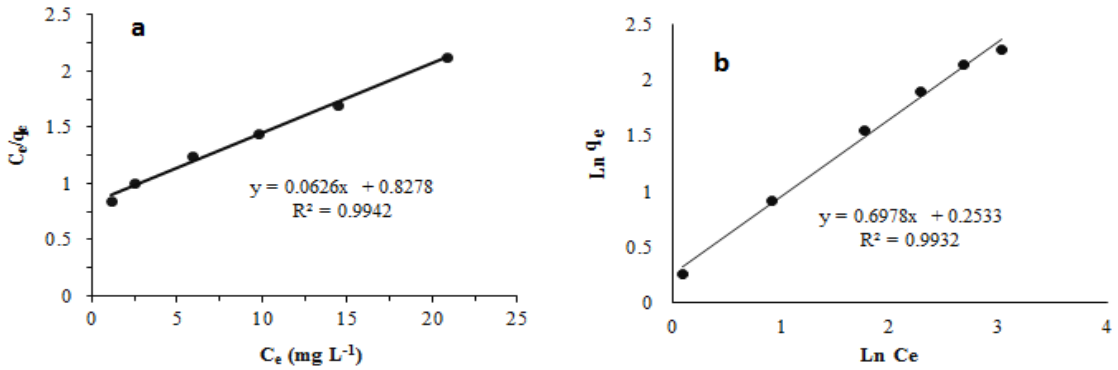

Fig. 10. Fitting the linear form of the (a) Redlich-Peterson and (b) Sips isotherms with the experimental data

Table 7. Parameters of two-parametric isotherms with linear and nonlinear regression methods

Adsorption model	Parameters	Unit	Isotherm	Nonlinear regression
Langmuir			$\frac{C_e}{qe}=\frac{1}{Q_{max}K_L}+\frac{1}{Q_{max}}C_e$	$qe=\frac{Q_{max}K_LC_e}{1+K_LC_e}$
	Q_{max}	Mg/g	16.2	16.61
	K_L	L/mg	0.074	0.07
	R^2	-	0.994	0.998
Freundlich		-	$\log qe=\log K_F+\frac{1}{n}\log C_e$	$qe=K_FC_e^{1/n}$
	K_F	$mg^{1-n}g^{-1}L^n$	1.26	1.55
	N	-	1.49	1.62
	R^2	-	0.994	0.988
Temkin		-	$\frac{C_e}{q_e}=\frac{1}{K_{RP}}+\frac{\alpha_{RP}}{K_{RP}}C_e{}^{\beta}$	$q_e=\frac{RT}{b}Ln(K_TC_e)$
	K_T	L/mg	1.1	1.1
	B	J g mg^{-2}	842.7	843.57
	R^2	-	0.96	0.965
Dubinin		-	$Lnq_e=LnQ_S-K_{ads}\varepsilon^2$	$q_e=Q_Sexp(-K_{ads}\epsilon^2)$
Radushkevich				
	K_{ads}	$mol^2\ J^{-2}$	$7*10^{-7}$	0.49
	Q_s	mol/g	6.8	0.78
	E	J/mol	845.1	1.01
	R^2	-	0.82	3.36

The fitting rates of the experimental data with nonlinear regression (q_e in terms of C_e) of Langmuir, Freundlich, Temkin, Redlich-Peterson, and sipsisotherms are plotted in Figure 11. As can be seen, the experimental data (blue circles) are highly consistent with the data from the nonlinear regression of Langmuir (brown circles), and in some places, they completely overlapped. Therefore, this comparison is also a confirmation of the Langmuir single-layer chemical adsorption mechanism.

Table 8. Parameters related to three-parametric isotherm with linear and nonlinear regression methods

Adsorption model	Parameters	Unit	Liner Regression	Nonlinear Regression
Redlich-Peterson			$\frac{C_e}{q_e}=\frac{1}{K_{RP}}+\frac{\alpha_{RP}}{K_{RP}}{C_e}^{\beta}$	$q_e=\frac{K_{RP}C_e}{1+\alpha_{RP}{C_e}^{\beta}}$
	K_{RP}	L/mol	1.31	1.35
	α_{RP}	L/g	0.13	0.06
	β	-	0.86	1.03
	R^2	-	0.993	0.998
Sips		-	$\beta LnC_e=-Ln\left(\frac{K_S}{q_e}\right)+Lna_S$	$q_e=\frac{K_S{C_e}^{\beta}}{1+\alpha_S{C_e}^{\beta}}$
	K_s	L/mg	1.95	1.89
	α_s	-	1.51	0.07
	β	-	0.69	0.98
	R^2	-	0.993	0.998

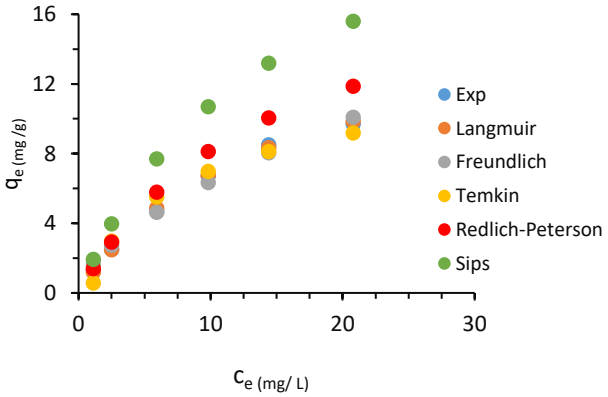

Fig.11. Fitting the nonlinear form of experimental data with different isotherms

3.3. Adsorption Kinetics

First-order, Pseudo-second-order, intra-particle diffusion, and mass transport models were used to investigate the nickel (II) adsorption kinetic with PPAP-MPTMS-MCM-41. To obtain the kinetic data, the time values of q at times of 2.5, 5, 10, 15, and 20 min were obtained using the remaining or equilibrium concentrations by the ICP-OES device and using the calibration curve according to Eq. (1). First, according to the first-order kinetic equation, the graph of this kinetic is plotted, as shown in Figure 12. The results show that the experimental data has no accordance with first-order kinetics. Therefore, it cannot be argued that the nickel (II) adsorption kinetic by the PPAP-MPTMS-MCM-41 adsorbent follows the first-order kinetic model.

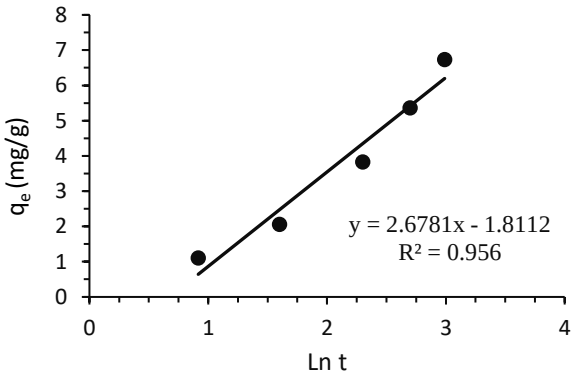

Fig. 12. Fitting the experimental data with first-order kinetics

The evaluation of the conformity of the experimental data with the pseudo-second-order kinetic model (Figure13) shows that the adsorption of nickel (II) ions by this modified nano-adsorbent and in this concentration is well compatible with pseudo-second-order kinetics. The kinetic parameters of both the first-order and Pseudo-second-order models are calculated and shown in Table 9.

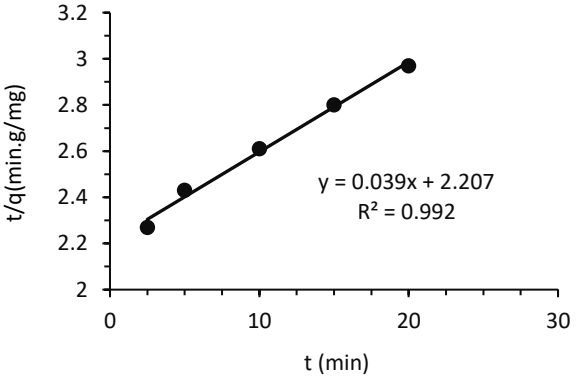

Fig. 13. Fitting of experimental data with the pseudo-second-order kinetics

Table 9. First-order and pseudo-second-order kinetics data

Kinetic model	Parameters	Value
First order	β	2.678
	α	0.19
	R^2	0.956
Pseudo second order	q_e (mg g)	25.64
	h (mg $g^{-1}min^{-1}$)	0.45
	K (g $mg^{-1}min^{-1}$)	$6.84*10^{-4}$
	R^2	0.992

Figure 14 presents the conformity of the intra-particle mass transfer model with the experimental data, the q_t diagram versus $t^{0.5}$, according to the experimental data. As can be seen, according to regression (R^2=0.994), the experimental data are highly consistent with the intra-particle mass transfer model. This conformity suggests that the nickel (II) ions should be able to easily penetrate the adsorbent nanoparticles after passing through the interface between the adsorbent and the solvent (common film) to interact with the adsorbent complexing sites.Based on the slope of the diagram, the value of the penetration coefficient of the nickel (II) ions inside the pores is equal to 1.96 mg g^{-1} $min^{-1/2}$. As can be inferred from this model, the q_t diagram versus $t^{0.5}$ must pass through the origin of the coordinates, but experimental data do not show such behavior. Therefore, this deviation from the intra-particle model explicitly states that in addition to the penetration of nickel (II) ions into the mesoporous cavities of PPAP-MPTM-MCM-41 (6.0 w w-1), other stages of mass transfer also play a role, and intra-particle diffusion is not the only mechanism of mass transfer.

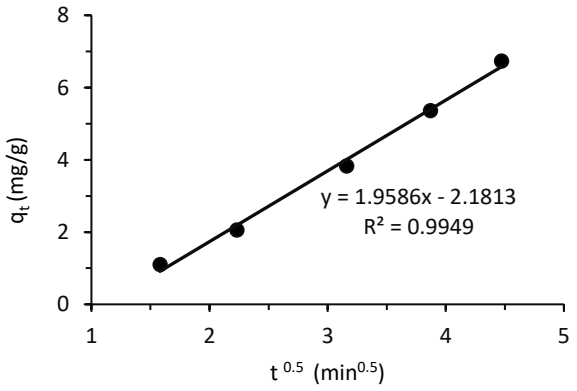

Fig. 14. Fitting of the experimental data with the intra-particle mass transfer model

3.4. Adsorption thermodynamic

The changes in the Gibbs free energy (ΔG^0) are the most important thermodynamic indicator that can be used to judge the degree of the spontaneity of a process. The changes in Gibbs free energy are related to the equilibrium constant according to:

$$\Delta G^0 = -RT \, Ln \, K_{eq} \quad (17)$$

where K_{eq} is the equilibrium constant, R is the universal gases constant, and T is the absolute temperature. ΔG^0 is usually expressed in units of (J/mol) [34].Also, Eq. 18 shows another expression that defines ΔG^0.

$$\Delta G^0 = \Delta H^0 - T\Delta S^0 \quad (18)$$

Therefore, by having changes in the Gibbs free energy for the adsorption of nickel (II) ions by this nano-absorber at different temperatures, the diagram ΔG^0 can be drawn versus temperature and ΔS^0, and ΔH^0 can be obtained using the slope and width of its intercept, respectively. To obtain ΔG^0 at different temperatures, the Langmuir isotherm, which had good conformity with the experimental data, in addition to ambient temperature (25℃), was plotted at temperatures of 35, 45, 55, and 65℃. The constant equilibrium values are given in Table 10.The value of ΔG^0 was calculated through Eq. (17) and used to draw the diagram ΔG^0 versus T. As can be seen in Figure 15, the ΔG^0 value of this adsorption process is positive and moves to lower values as the temperature increases. Therefore, it suggests that as the temperature increases, the process progresses to a spontaneous process. According to the slope and intercept of the graph, the values of ΔH^0 and ΔS^0 were 32185(J/mol) and 86.7 (J $mol^{-1}k^{-1}$), respectively. The positive values of these two important thermodynamic parameters indicate that the process of adsorption of nickel ions by this modified nano-adsorbent is endothermic, and the entropy in the solution-nano-adsorbent interface increases.

Table 10. Standard Gibbs free energy data at different temperatures

Temp, K	K_L,(L/mg)	ΔG^0,(J/mol)
298	0.074	6450.8
308	0.122	5393.4
318	0.18	4533.7
328	0.262	3650.5
338	0.345	2985.5

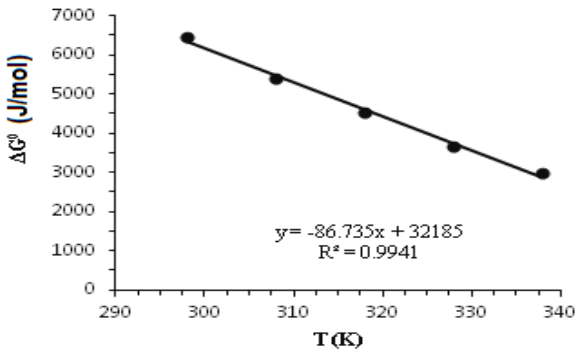

Fig. 15. The changes in Gibbs free energy versus absolute temperature

4. Conclusions

In this study, a PPAP-MPTMS-MCM-41 nano-adsorbent was used for the adsorption of nickel (II) ions in a batch process.

The parameters effective in this adsorption process, as well as kinetic, thermodynamic, and mass transfer studies, were investigated, and the following results were obtained.

1. Studying the parameters affecting adsorption showed that the PPAP-MPTMS-MCM-41 adsorbent is most effective in the adsorption of nickel (II) under the following conditions: pH =8, contact time = 20 min, 6 wt.% of PPAP ligand, adsorbent mass = 0.3 g, 1 molar hydrochloric acid (to remove nickel from the adsorbent), and NaCl salt with a concentration of less than 100 g/L.
2. Two-parametric and three-parametric isotherms were investigated under optimal conditions and found that the experimental data are in good conformity with the Langmuir adsorption isotherm model.
3. The study of the kinetic models and mass transfer of this adsorption process showed that the experimental data are in good conformity with the pseudo-second-order and the intra-particle diffusion mass transfer kinetic models.
4. Thermodynamic studies showed that ΔG^0 is positive, and this process is endothermic such that as the temperature rises, it goes to lower values. As a result, the process progresses to a spontaneous process as the temperature rises.

References

[1] Duda-Chodak A, Blaszczyk U. (2008). The impact of nickel on human health. *Journal of elementology*, *13*(4),685-693.

[2] Badruddoza A, Tay A, Tan P, Hidajat K, Uddin M. (2011). Carboxymethyl-β-cyclodextrin conjugated magnetic nanoparticles as nano-adsorbents for removal of copper ions: synthesis and adsorption studies. *Journal of hazardous materials*, *185*(2-3),1177-1186.

[3] Song J, Kong H, Jang J. (2011). Adsorption of heavy metal ions from aqueous solution by polyrhodanine-encapsulated magnetic nanoparticles. *Journal of colloid and interface science*, *359*(2),505-511.

[4] Khan TA, Singh VV. (2010). Removal of cadmium (II), lead (II), and chromium (VI) ions from aqueous solution using clay, *Toxicological and environ chemistry 92*(8),1435-1446.

[5] Subramani BS, Shrihari S, Manu B, Babunarayan K. (2019). Evaluation of pyrolyzed areca husk as a potential adsorbent for the removal of Fe^{2+} ions from aqueous solutions. *Journal of environmental management*, *246*,345-354.

[6] Abadi MJ, Nouri S, Zhiani R, Heydarzadeh H, Motavalizadehkakhky A. (2019). Removal of tetracycline from aqueous solution using Fe-doped zeolite. *International journal of industrial chemistry*, *10*(4),291-300.

[7] Mousavi SZ, Manteghian M, Shojaosadati SA, Pahlavanzadeh H. (2018). Keratin nanoparticles: synthesis and application for Cu (II) removal. *Advances in Environmental Technology*, *4*(2), 83-93.

[8] Sharaf G, Abdel-Galil E, El-eryan Y. (2018). Modeling studies for adsorption of phenol and co-pollutants onto granular activated carbon prepared from olive oil industrial waste. *Advances in environmental technology*, *4*(1),23-40.

[9] Schulz-Ekloff G, Wöhrle D, van Duffel B, Schoonheydt RA. (2002). Chromophores in porous silicas and minerals: preparation and optical properties. *Microporous and mesoporous materials, 51*(2),91-138.

[10] Scott BJ, Wirnsberger G, Stucky GD. (2001). Mesoporous and mesostructured materials for optical applications. *Chemistry of materials*, *13*(10),3140-3150.

[11] Moriguchi I, Honda M, Ohkubo T, Mawatari Y, Teraoka Y. (2004). Adsorption and photocatalytic decomposition of methylene blue on mesoporous metallosilicates. *Catalysis today*, *90*(3-4),297-303.

[12] Adjdir, M. (2010). *Synthesis of mesoporous nanomaterials from natural sources as low-cost nanotechnology* (Doctoral dissertation, Verlag nicht ermittelbar).

[13] Øye G, Sjöblom J, Stöcker M. (2001). Synthesis, characterization and potential applications of new materials in the mesoporous range. *Advances in colloid and interface science*, *89*,439-466.

[14] Pinnavaia T. (1999). Selective adsorption of Hg^{2+} by thiol-functionalized nanoporous silica. *Chemical communications*, (1), 69-70.

[15] Liu AM, Hidajat K, Kawi S, Zhao DY. (2000). A new class of hybrid mesoporous materials with functionalized organic monolayers for selective adsorption of heavy metal ions. *Chemical communications*, (13), 1145-1146.

[16] Algarra M, Jiménez MV, Rodríguez-Castellón E, Jiménez-López A, Jiménez-Jiménez J. (2005). Heavy metals removal from electroplating wastewater by aminopropyl-Si MCM-41. *Chemosphere*, *59*(6), 779-786.

[17] Ebrahimzadeh H, Tavassoli N, Sadeghi O, Amini M, Vahidi S, Aghigh SM, Moazzen E. (2012). Extraction of nickel from soil, water, fish, and plants on novel pyridine-functionalized MCM-41 and MCM-48 nanoporous silicas and its subsequent determination by FAAS. *Food analytical methods*, *5*(5),1070-1078.

[18] Ghorbani M, Nowee SM. (2015). Kinetic studies of Pb and Ni adsorption onto MCM-41 amine-functionalized nano particle. *Advances in environmental technology*, *1*(2), 101-104.

[19] He R, Wang Z, Tan L, Zhong Y, Li W, Xing D, Wei C, Tang Y. (2018). Design and fabrication of highly ordered ion imprinted SBA-15 and MCM-41 mesoporous

organosilicas for efficient removal of Ni2+ from different properties of wastewaters. *Microporous and mesoporous materials*, *257*,212-221.

[20] Northcott KA, Miyakawa K, Oshima S, Komatsu Y, Perera JM, Stevens GW .(2010). The adsorption of divalent metal cations on mesoporous silicate MCM-41. *Chemical engineering journal*, *157*(1),25-28.

[21] Jalali M, Aliakbar A. (2013). Electrochemical synthesis and characterization of a new selective chelating agent for Ni (II) and its environmental analytical application. *Analytical methods*, *5*(22),6352-6359.

[22] Aliakbar A, Jalali M. (2014). Electrosynthesis of a new selective chelating agent for solid phase extraction of Ni (II) from water samples: characterisation and analytical applications. *International journal of environmental analytical chemistry*, 94(6),562-578.

[23] Teymouri M, SAMADI MA, Vahid A. (2011). A rapid method for the synthesis of highly ordered MCM-41 *International Nano Letters*, 1(1),34-37.

[24] Jalali M, Aliakbar A. (2015). Synthesis, characterisation and application of mercapto- and polyaminophenol-bifunctionalised MCM-41 for dispersive micro solid phase extraction of Ni(II) prio to inductively coupled plasma-optical emission spectrometry (DMSPE-ICP-OES). *International journal of environmental analytical chemistry*, *95*(6),542-555.

[25] Showkat AM, Zhang Y-p, Kim MS, Gopalan AI, Reddy KR, Lee K. (2007). Analysis of heavy metal toxic ions by adsorption onto amino-functionalized ordered mesoporous silica. *Bulletin-Korean chemical society*, *28*(11),1985.

[26] Khosa MA, Ullah A. (2014). In-situ modification, regeneration, and application of keratin biopolymer for arsenic removal. *Journal of hazardous materials*, *278*,360-37.

[27] Freundlich H. (1906). Uber die adsorption in losungen [Adsorption in solution]" *Zeitschrift für physikalische chemie*, 57, 384-470.

[28] Langmuir I. (1916). The constitution and fundamental properties of solids and liquids. Part I. Solids. *Journal of the American chemical society*, *38*(11),2221-2295.

[29] Ayawei N, Ebelegi AN, Wankasi D. (2017). Modelling and interpretation of adsorption isotherms. *Journal of chemistry*, *2017 (11),1-11.*

[30] Redlich O, Peterson DL. (1959). A useful adsorption isotherm. *Journal of physical chemistry*, *63*(6),1024-1024.

[31] Sips R .(1948). On the structure of a catalyst surface. *The journal of chemical physics*, *16*(5),490-495.

[32] Qiu, H., Lv, L., Pan, B. C., Zhang, Q. J., Zhang, W. M., Zhang, Q. X. (2009). Critical review in adsorption kinetic models. *Journal of Zhejiang University-Science A*, *10*(5), 716-724.

[33] Pérez-Quintanilla D, Sánchez A, del Hierro I, Fajardo M, Sierra I. (2007). Preparation, characterization, and Zn2+ adsorption behavior of chemically modified MCM-41 with 5-mercapto-1-methyltetrazole. *Journal of colloid and interface science*, *313*(2),551-562.

[34] Aksu Z. (2002). Determination of the equilibrium, kinetic and thermodynamic parameters of the batch biosorption of nickel (II) ions onto Chlorella vulgaris. *Process biochemistry*, *38*(1),89-99.